FINITE ELEMENT SIMULATION OF COMPRESSION BEHAVIOR OF CELLULAR METALS

Renato V. Linn
Branca F. de Oliveira
natofox@hotmail.com
branca@ufrgs.br
Virtual Design Research Group -ViD, Universidade Federal do Rio Grande do Sul
Av. Osvaldo Aranha, 99, 4° andar, 90035-190, Porto Alegre – RS – Brazil.

Abstract. *Metal foams are materials of recent development and application that show interesting combinations of physical and mechanical properties. Foams are commonly used as equipments of passive safety due to their high capacity of energy absorption under impact conditions. Considering that compression is the dominant loading in impact situations, in this work a finite deformation simulation of a compression test on a cellular metal sample including damage effects and self-contact is shown.*
The damage analysis in metallic foams is a complex problem and must be performed in a finite strain context. The self-contact problem is analyzed through symmetry contact hypothesis, which provide a considerable reduction in the computational cost.
The main objective of this work is to characterize the behavior of a cellular metal in compression using a combination of the internal buckling effects shown by the structure. The RVE concept is used and considering three different deformed shapes for the former cells in the compressed cellular body the overall behavior is represented, according to the number of cells in the structure. The number of cells determines the configuration of the localized bucking effects in the cellular microstructure.

Keywords: *Cellular Metals, Metallic Foams, Damage, Gurson Models, Finite elements*

1. INTRODUCTION

This work continues the research on the simulation of metallic foams behavior that was presented in earlier papers (Oliveira et al., 2008, 2007 and 2006).

We understand by metal foam a material composed by a metallic matrix with internal voids (Fig. 1). Metallic foams are increasingly used by the automotive industry, particularly as recourse of passive safety. In that case, they act to absorb impact energy.

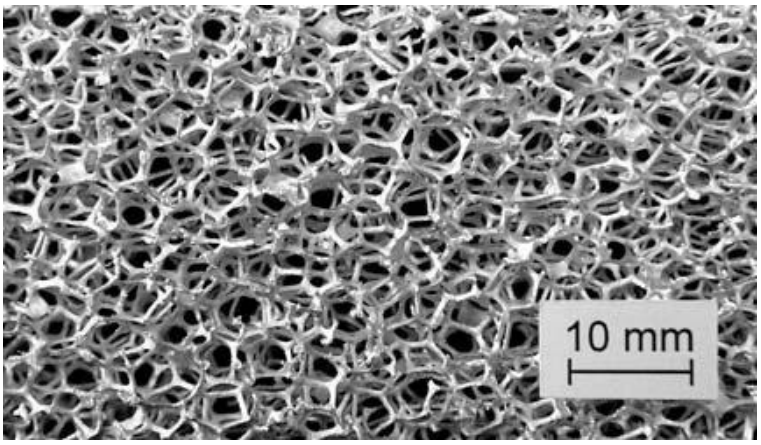


Figure 1- Aluminum foam with open cell (DUOCEL®) (Öchsner and Lamprecht, 1999).

Metallic foams show mechanical behavior and physical properties that strongly differ from those of solid materials and show interesting combinations of properties. For example, high stiffness combined with low specific weight, or permeability to gas flow combined with high thermal conductivity, offering possibilities of use in aerospace and automotive industries. The schematic stress-strain curve for a metallic foam in compression (Fig. 2), shows a large area in the plateau region corresponding to high energy absorption at constant stress.

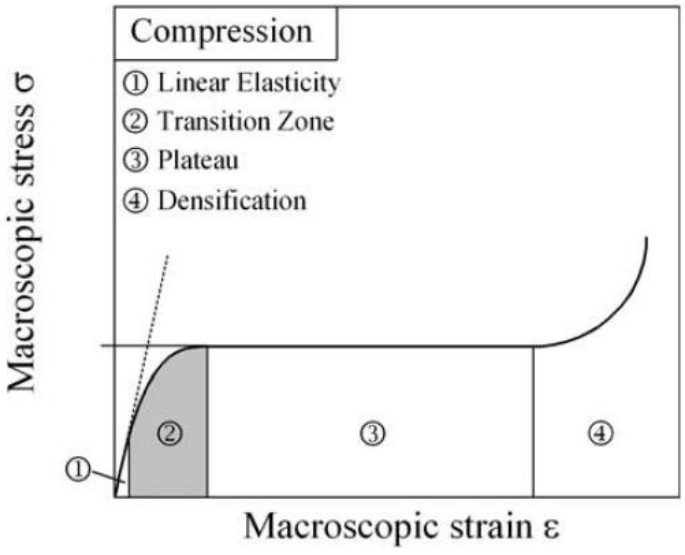


Figure 2- Stress-strain curve for a foam showing large capacity of energy absorption at constant stress (Öchsner et al., 2003).

2. GURSON DAMAGE MODEL

The Gurson damage model was developed to describe the mechanical effect of high plastic deformations in ductile metals. The loss of resistance is governed by the porosity level. The (isotropic) damage variable employed is the volumetric void fraction, represented by f and defined by $f = V_V / V$, where V_v is the volume of voids in a representative small volume V, corrected for effects as stress concentration, etc.; f is defined at each point of the continuum. The presence of voids alters the elastoplastic constitutive relations. The equations usually employed in computational damage analyses, the Gurson-Tvergaard model (Gurson, 1977), (Tvergaard, 1981), considers a yield surface defined by.

$$\Phi = \sqrt{\frac{3}{2} S_{ij} S_{ij}} - \bar{\omega}\sigma_y = 0 . \tag{1}$$

where

$$\bar{\omega} = \left[1 - 2\alpha_1 f \cosh\left(\frac{\alpha_2 3p}{2\sigma_y} \right) + \alpha_3 f^2 \right]^{1/2} . \tag{2}$$

$$S_{ij} = \sigma_{ij} - p\delta_{ij} . \qquad p = \tfrac{1}{3}\sigma_{ij}\delta_{ij} . \tag{3}$$

$$\alpha_1 = \frac{1}{f_U} = 1.5 . \qquad \alpha_2 = 1.0 . \qquad \alpha_3 = \alpha_1^{\,2} . \tag{4}$$

and σ_{ij} are the Cauchy stresses, σ_y the yield stress in simple tension. α_i are material parameters. The parameter $f_U = 1/\alpha_1$ is the maximum volumetric void fraction admissible before rupture in absence of pressure. Another possible interpretation for the α_1 and α_2 parameters is that they work as multipliers acting on porosity f and pressure p, respectively.

In Fig. 3, yield surfaces for different levels of void content are shown, in a plot of normalized deviatoric stress versus normalized pressure.

It can be seen that the plastic domain depends on the hydrostatic pressure. When the volumetric void fraction f decreases, decreases the influence of pressure, leading to a larger elastic domain. For $f = 0$, the model reduces to the von Mises model, which is independent of hydrostatic pressure. It should be noted here that in the absence of hydrostatic pressure, the coefficient $\bar{\omega}$ reduces to:

$$\bar{\omega} = 1 - \alpha_1 f = 1 - \frac{f}{f_U} . \tag{5}$$

The plastic strain rate tensor is given by

$$D_{ij}^{\,p} = \dot{\lambda} \frac{\partial \Phi}{\partial \sigma_{ij}} . \tag{6}$$

And the equivalent plastic strain rate is defined by

$$\dot{\varepsilon}^p = \sqrt{\tfrac{2}{3} D_{ij}{}^p D_{ij}{}^p} \ . \tag{7}$$

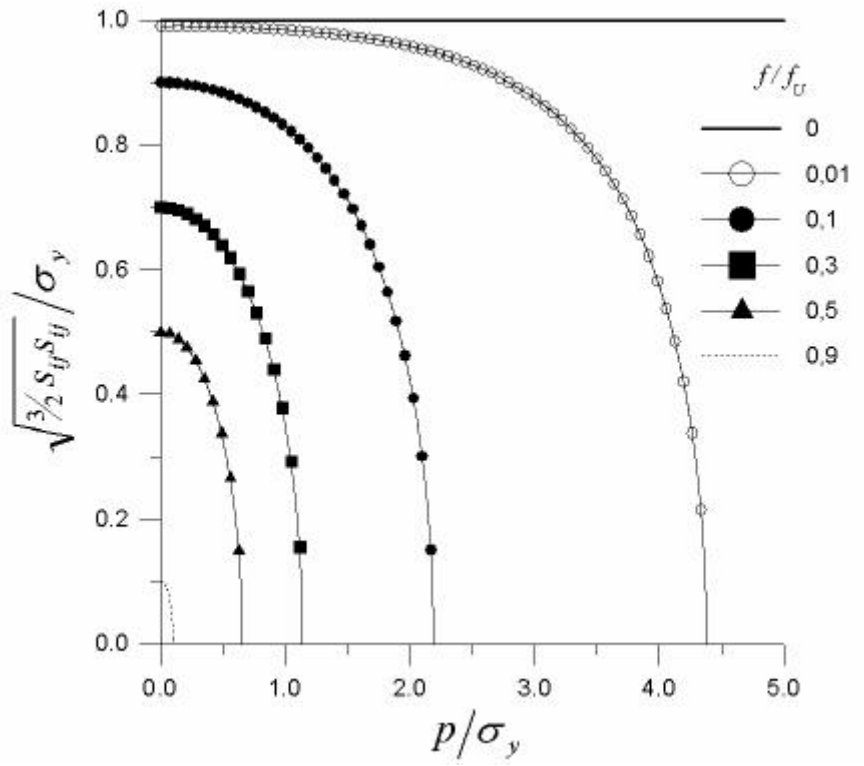


Figure 3- Yield surface for a porous material: influence of volumetric void fraction.

The basic mechanisms of damage evolution are nucleation, growth and coalescence of voids. Nucleation occurs mainly due to material defects, in the presence of tension. Growth occurs when the voids (preexistent or nucleated) change their size according to the volume change in the continuum.

Coalescence is related to the fast rupture process that occurs after that the volumetric void fraction reaches a limit, indicated by f_C. Coalescence consists in the union of neighbor voids due to the rupture of a ligament.

The equations that govern damage evolution are modeled in a simplified form as follows. First, it is assumed that total void rate is given by

$$\dot{f} = \begin{cases} \dot{f}_n + \dot{f}_g & f \le f_C \\ \dot{f}_C & f > f_C \end{cases} \tag{8}$$

where $\dot{f}_n$ is the void nucleation rate, $\dot{f}_g$ is the void growth rate and $\dot{f}_C$ is the void coalescence rate. Thus, as long as f is smaller than a characteristic value f_C only nucleation and growth develop. Above f_C, only coalescence takes place.

The nucleation rate is proportional to the rate of equivalent plastic strain

$$\dot{f}_n = A(\varepsilon^p)\dot{\varepsilon}^p . \tag{9}$$

The statistical distribution proposed for $A(\varepsilon^p)$ (Chu and Needleman, 1980)

$$A(\varepsilon^p) = \frac{f_N}{S_N\sqrt{2\pi}} \exp\left[-\frac{1}{2}\left(\frac{\varepsilon^p - \varepsilon^N}{S^N}\right)^2\right]. \tag{10}$$

where f_N is the nucleation void volumetric fraction, ε_N is the plastic strain value for nucleation and S_N is the standard deviation for the distribution. Sometimes it is assumed that nucleation takes place only in tension (Cunda and Creus, 1990), (ABAQUS Theory Manual, 1992) what implies that

$$A(\varepsilon^p) = 0 \quad \text{if} \quad p < 0 . \tag{11}$$

Growth rate of voids is controlled by mass conservation through the expression

$$\dot{f}_g = (1-f)D_{ii}{}^p . \tag{12}$$

Voids increase or decrease their volume according to the volume variation in the continuum. Coalescence is governed (Tvergaard, 1982) by the relation

$$\dot{f}_C = \frac{f_U - f_C}{\Delta\varepsilon}\dot{\varepsilon}^p . \tag{13}$$

Or in a alternative way (Tvergaad, 1981), (ABAQUS Theory Manual, 1992) employing in Eq. (2) a corrected volumetric void fraction given by

$$f^* = \begin{cases} f \\ f_C\,(1.0\,f_C)(f - f_C)/\,f_p\,f_C \end{cases} \tag{14}$$

In this case, only nucleation and growth are considered in Eq. (8).

The commercial finite element code ABAQUS is used in this work and the Gurson damage model is one of the available constitutive relationships.

3. MODELING CONSIDERATIONS FOR METTALIC FOAMS

Metal foam properties can change along the production process, particularly according to the cell being open or closed and the relative density of the foam in relation to the base material. Moreover, foams show (see Fig. 1) a fairly random structure. It is possible to determine the exact geometry using CT-scan (computed tomography) and model it with a dense mesh of finite elements, as in Fig 4-a. A different approach towards the understanding and modeling of these materials, adopted in this work, is an idealization as a cellular material with regular structure, as in Fig. 4-b. In this case, modeling a RVE (representative volume element, Fig. 4-c) and still considering the existent symmetries, good results can be obtained with fewer elements. Then, specimens with regular structure may be tested to validate results and determine material parameters. These homogenization procedures have been used with

success in other areas of continuum mechanics. A specimen of a cellular metal made to represent a foam is shown in Fig. 5.

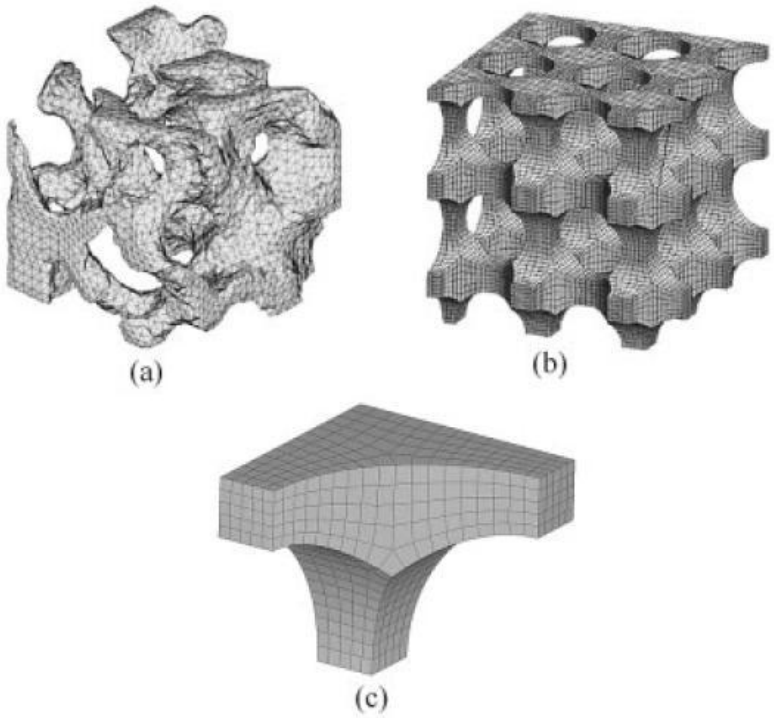


Figure 4- Meshes used to represent a cellular metal (Öchsner and Lamprecht, 2003).

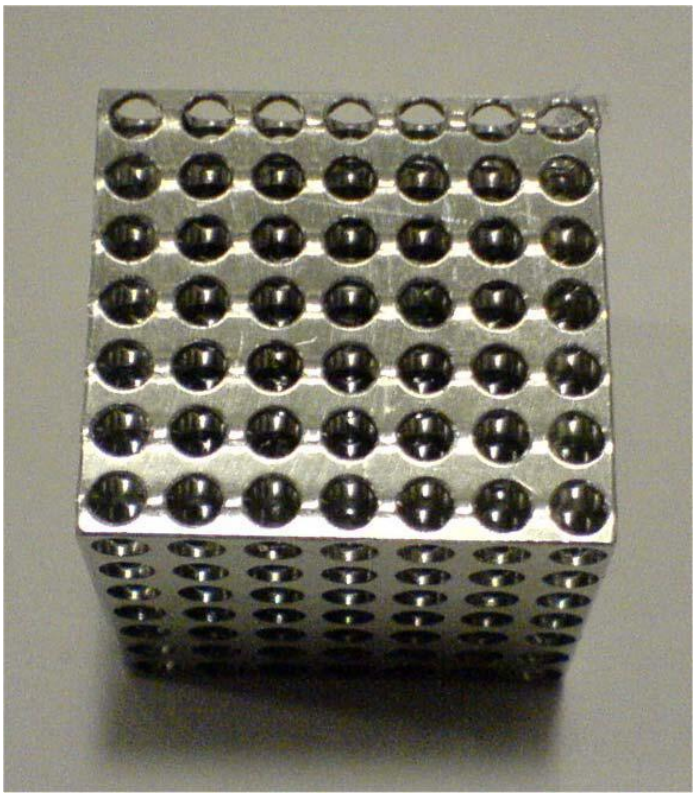


Figure 5- Cube of cellular metal.

3.1 Application of boundary conditions

One important aspect to take into account when modeling cells as those described above are the boundary conditions, that must represent the average behavior of the foam. When a vertical displacement is applied to the top side (see Fig. 6) the vertical faces must continue vertical while the distance between them may change.

This behavior can be computationally imposed using multiple point constraints (MPC). The used FE code (ABAQUS) offers the possibility to realize such a boundary condition where all nodes on a certain surface have the same x-displacement: $u_{xi} = ... = u_{xj}$. The effect of differing boundary conditions on the deformation is shown in Fig. 6

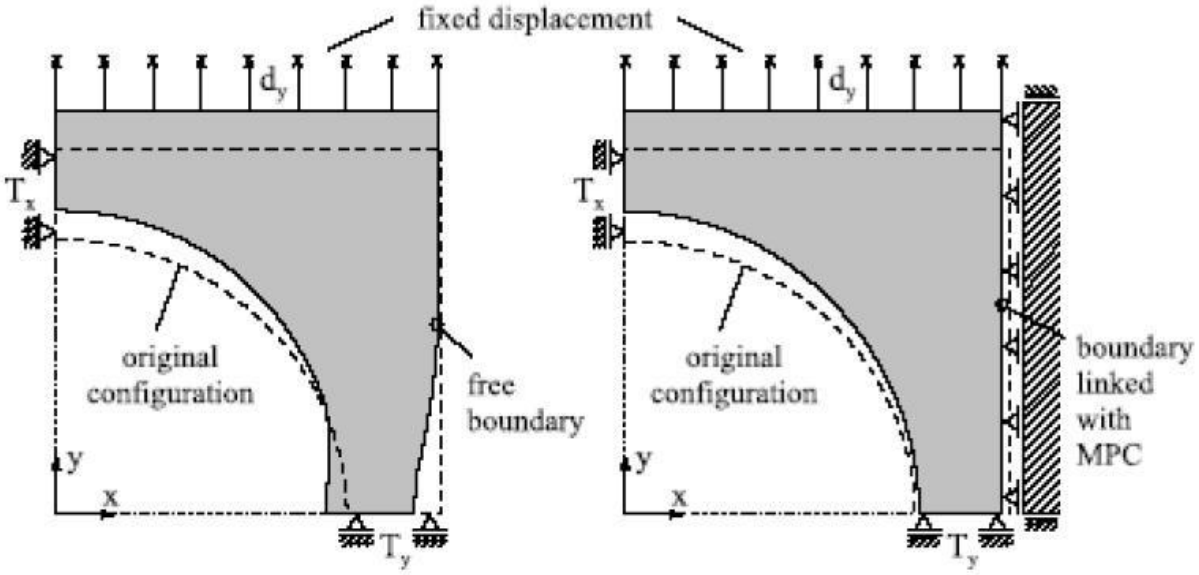


Figure 6- Results of different boundary conditions applied to the right face (Öchsner and Lamprecht, 1999).

3.2 Contact hypothesis and formulation

Considering the contact between each part of the cellular metal perfect, the implementation of the self-contact can be imposed by the symmetry of the contact.

Considering a rigid infinite plane disposed on xy plane between a unit cell and its adjacent unit cell of the cellular metal, and a single point "P_0" on the surface of the unit cell with coordinates $\left(\vec{i}_0, \vec{j}_0, \vec{k}_0\right)$ that have a load or displacement applied in the z axis. This point will have contact with a point on the surface of the adjacent cell, "P_n", with coordinates $\left(\vec{i}_0, \vec{j}_0, \vec{k}_{0+n}\right)$ that becomes $\left(\vec{i}_0, \vec{j}_0, -\vec{k}_0\right)$ due to the symmetry, if this coordinates are the relatives coordinates from the plane that stands symmetric between this cells. Also, the point of contact is equal to the plane coordinates $\left(\vec{i}_0, \vec{j}_0, 0\right)$, Fig. 7.

This hypothesis can be extended considering 6 planes that enclosure a unit cell with its neighborhoods cells at every 3-d space direction. In another words, the contact occurs where two points touch a plane.

The advantage of the use of this kind of contact is that a deformable finite element mesh with self-contact is replaced by a single deformable finite element mesh with contact with rigid bodies (planes), which needs much less computational work and have better convergence range.

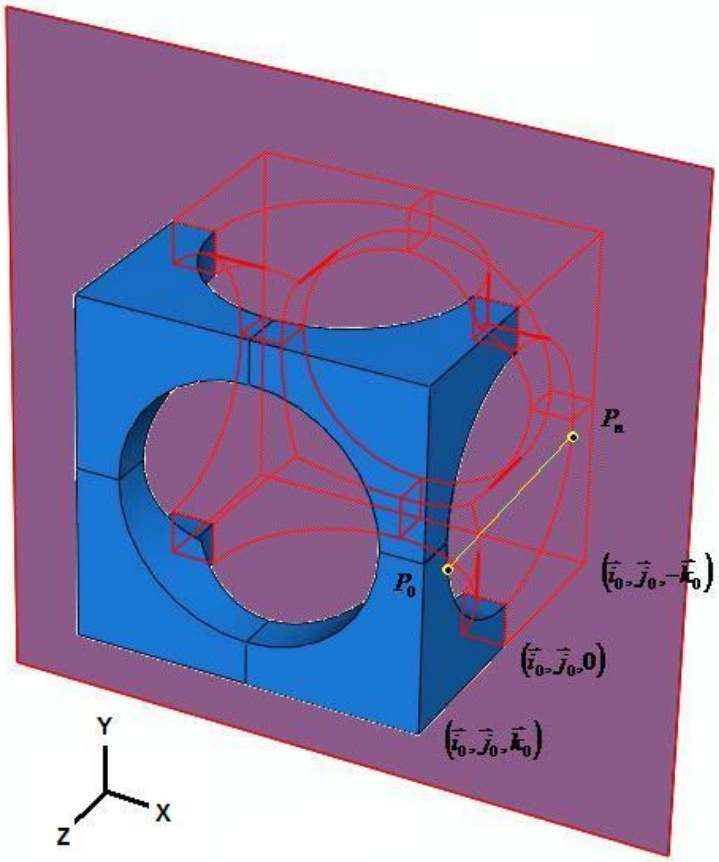


Figure 7- Contact hypothesis example for a load on z direction.

The used FE code (ABAQUS) provides a formulation for modeling the interaction between a deformable body and an arbitrarily shaped rigid body that may moved during the analysis. It is used finite-sliding formulation where separation and sliding of finite amplitude and arbitrary rotation of the surfaces may arise. The finite-sliding rigid contact capability is implemented by means of a family of contact elements that ABAQUS automatically generates based on the data associated with the user-specified contact pairs. At each integration point these elements construct a measure of overclosure (penetration of the point on the surface of the deforming body into the rigid surface) and measures of relative shear sliding. These kinematic measures are then used, together with appropriate Lagrange multiplier techniques, to introduce surface interaction theories (contact and friction).

The contact formulation is given by

$$nh = -x_A + x_C + r\,. \tag{15}$$

where x_A is the coordinate of a point x_A on the deforming mesh, x_C is the coordinate of the rigid body reference node C, A' is the closest point of A on the surface of the rigid body at which the normal to the surface of the rigid body, *n*, passes (from A' to *A*), *r* is the vector

from C to A' and h is the "overclosure" of the surfaces, given by the distance from A' to A along $-n$. The geometry described by these quantities is shown in Fig. 8.

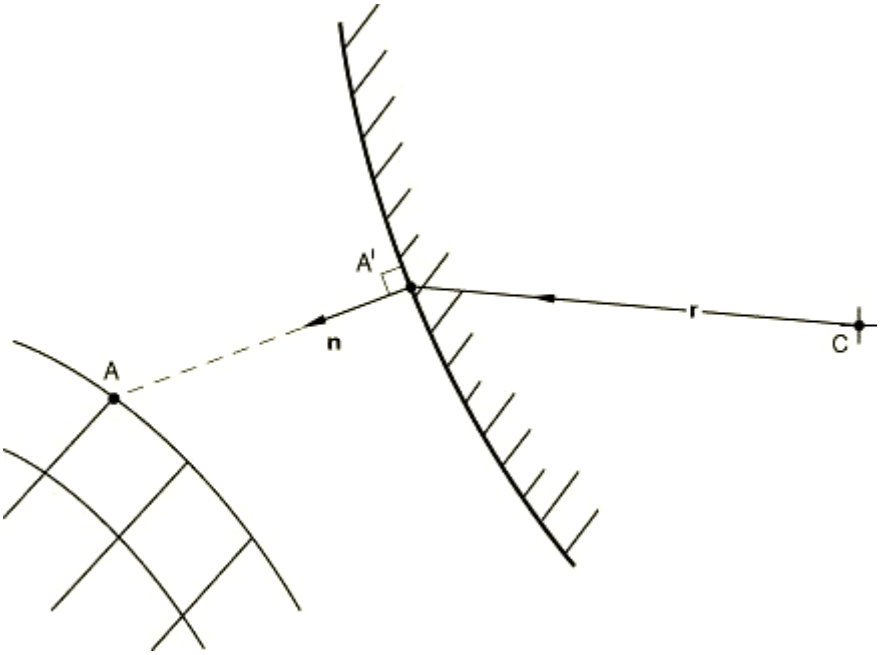


Figure 8- Rigid surface interface geometry (ABAQUS Theory Manual, 1992).

Then if $h < -c$ there is no contact between the surfaces at A, and no further surface interaction calculations need to be done at this point, where c is the clearance below which contact occurs. The used clearance is $c = 0$, a "hard" surface.

To enforce the contact constrain, the first variation of h, δh and its second variation, $d\delta h$ are also needed, and (for a "hard" contact)

$$\delta h = -n(\delta x_A - \delta x_C) + (r \times n) \cdot \delta\phi_C . \tag{16}$$

$$\begin{aligned} d\delta h = {} & (n \cdot r)\delta\phi_C \cdot d\phi_C - \frac{1}{2}\delta\phi_C \cdot (nr + rn) \cdot d\phi_C + \delta\phi_C \cdot (t_\alpha \times n) d\gamma_\alpha \\ & + d\phi_C \cdot (t_\alpha \times n)\delta\gamma_\alpha + \delta\gamma_\alpha n \cdot \kappa_{\alpha\beta} d\gamma_\beta . \end{aligned} \tag{17}$$

where δx_i and $\delta\phi_i$ are the first variation of the displacement and rotation of the point i, and $d\delta x_i$ and $d\delta\phi_i$ are the second variation of the displacement and rotation of the point i, respectively. The term $\delta\gamma_\alpha$ is the "slip" of point A' and S^α ($\alpha = 1.2$) is the locally orthogonal distance measuring surface coordinates on the surface at A'. The S^α measure distance along the tangents t_α to the surface at A', also, $d\gamma_\alpha$ is its variation and the term $\kappa_{\alpha\beta}$ is the surface curvature matrix, given by

$$\kappa_{\alpha\beta} = \frac{\partial t_\alpha}{\partial S_\beta} = \frac{\partial t_\beta}{\partial S_\alpha} = \frac{\partial^2 r}{\partial S_\alpha \partial S_\beta} . \tag{18}$$

The "hard" contact assumed that

$$h = \delta h = dh = 0. \tag{19}$$

and also

$$d\delta x_A = d\delta x_C = d\delta \phi_C = 0. \tag{20}$$

The expression involving $\kappa_{\alpha\beta}$ can be simplified somewhat, because $n \cdot t_\alpha = 0$, hence

$$n \cdot \kappa_{\alpha\beta} = n \cdot \frac{\partial t_\alpha}{\partial S_\beta} = -t_\alpha \cdot \frac{\partial n}{\partial S_\beta} = t_\beta \cdot \frac{\partial n}{\partial S_\alpha}. \tag{21}$$

similarly

$$t_\gamma \cdot \kappa_{\alpha\beta} = t_\gamma \cdot \frac{\partial t_\alpha}{\partial S_\beta} = -t_\alpha \cdot \frac{\partial t_\gamma}{\partial S_\beta}. \tag{22}$$

4. SIMULATION OF A COMPRESSION TEST ON A CUBE OF CELLULAR METAL

A cube of cellular metal as shown in Fig. 5 is considered in the following. The cube contains $3mm$ diameter holes with distance of $4mm$ among them. The presence of holes simulates a cellular metal with relative density of 0.2712.

The matrix material properties are $E = 72.7GPa$, $\nu = 0.34$, initial yield value ${\sigma_y}^0 MPa = 250MPa$ and final yield value ${\sigma_y}^\infty MPa = 410MPa$ (Fig. 9). Hardening is taken into account by the relation $\sigma_y = \sigma_y^0 + \left(\sigma_y^\infty - \sigma_y^0\right)\left[1 - \exp\left(-k\varepsilon^p\right)\right]$, with $k = 25$. The Gurson model of the ABAQUS code is used and the parameters considered are 5% of initial porosity, $\alpha_1 = 1.5$ and $\alpha_2 = 1.5$. The material parameters are obtained fitting experimental results. (Öchsner and Lamprecht, 2003), (Munoz-Rojas et al., 2007).

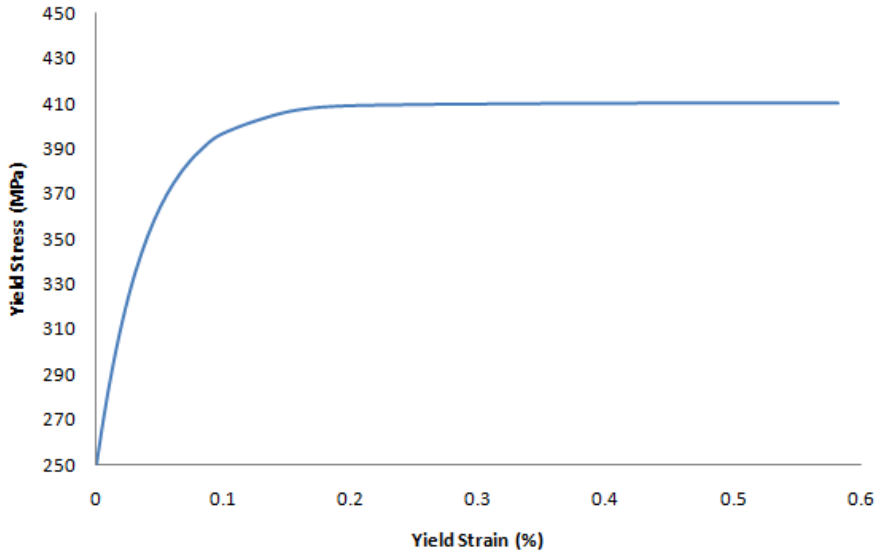


Figure 9- Stress strains plots for the plastic deformation on the cellular metal material.

Load is applied as a vertical displacement on the top surface of the cube.

The objective of this analysis is to characterize the behavior of a cellular metal in compression according to the number of cells in the structure.

Five models are used to simulate the problem, beginning with a single cell as shown in Fig. 10-a, and varying the number of cells in each direction and the boundary conditions. The single cell model of Fig. 10-a is studied with and without MPC boundary conditions (see Fig. 6) in three different conditions: with MPC applied to the two faces parallel to the applied load (called BCK-0 here), with MPC applied to one face parallel to the applied load (called BCK-1 here) and without MPC (called BCK-2 here). The number of those denominations is a reference to the number of walls free to show a buckling effect. With 2 cells in each direction the model called 2-cells (Fig. 10-b) is obtained, representing a cube with a single hole. Employing 4 cells in each direction the models called 4-cells is obtained (Fig. 10-c).

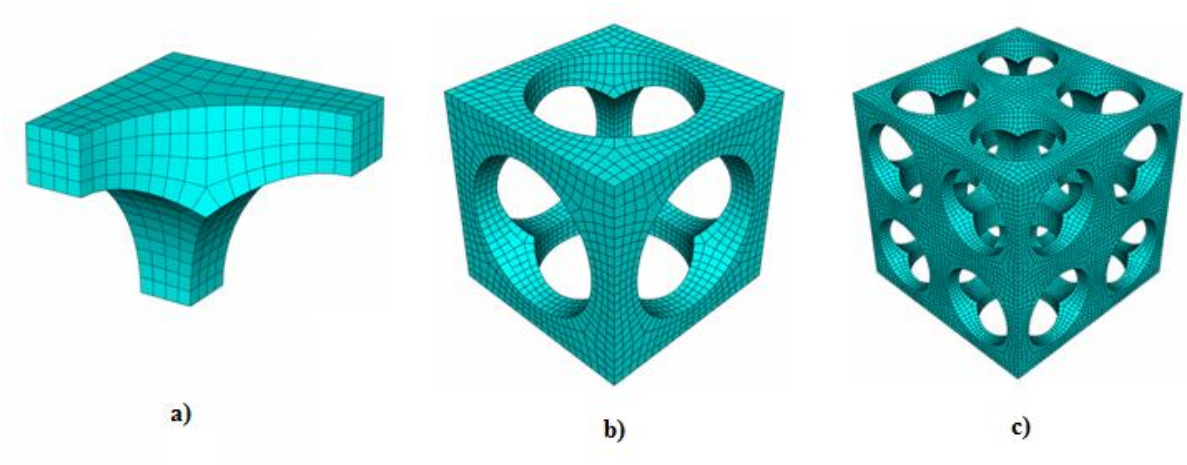


Figure 10- Meshes used to study the cube. a) unit cell b) 2-cells c) 4-cells.

Figure 11 shows a comparison among macroscopic stress and strain plots for the five models used in the analysis (three types of unit cell, a 2-cells and a 4-cells) and an experimental specimen. The macroscopic stress is the relation between the resultant forces and the original solid surface area. The macroscopic strain is the ratio between change of length and original length. It can be seen that the first unit cell analysis BCK-0 (Fig. 10-a) with MPC applied to two faces overestimates the stiffness of the model. Using MPC, due to the nature of the restriction (see section 3.1), both of the side walls remain vertical. This effect is more significant after 2.5% macroscopic strain, when buckling occurs in the walls between the holes (Fig. 12). Figure 13 shows the von Mises stress distribution for the unit cell with MPC BCK-0 at an applied macroscopic strain of 25% (Fig. 13-a) and 50% (Fig. 13-b).

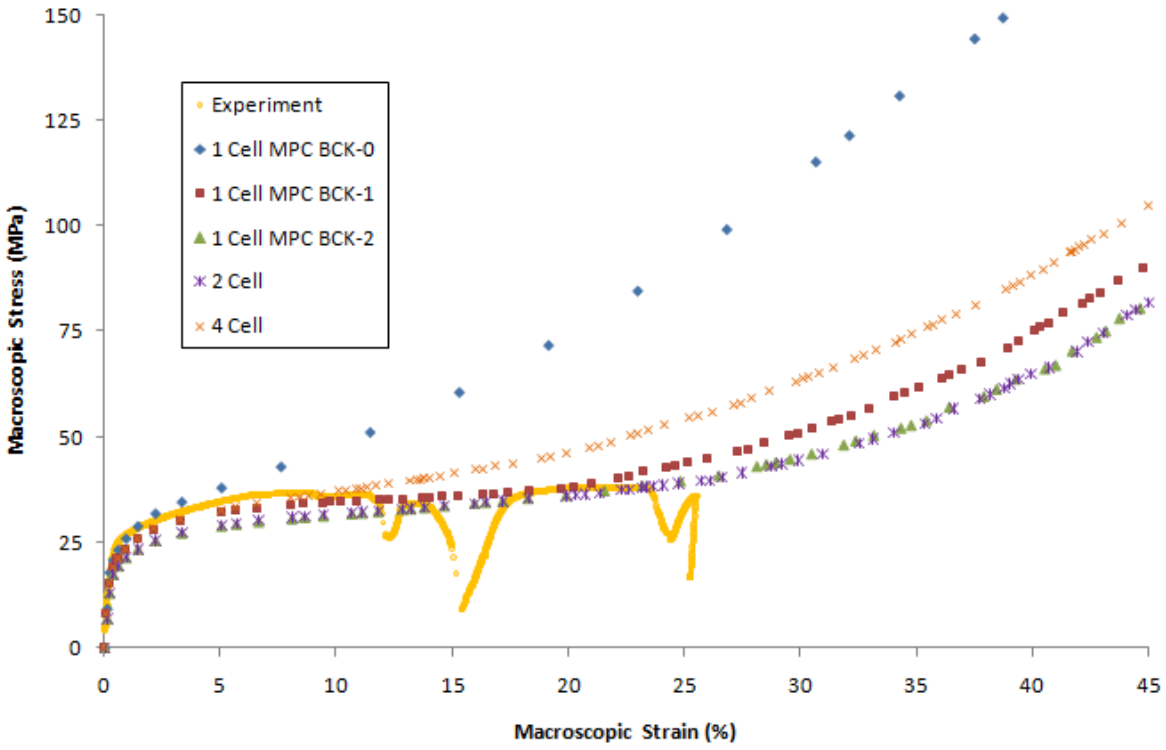


Figure 11- Stress strain plots for the models used in the analysis.

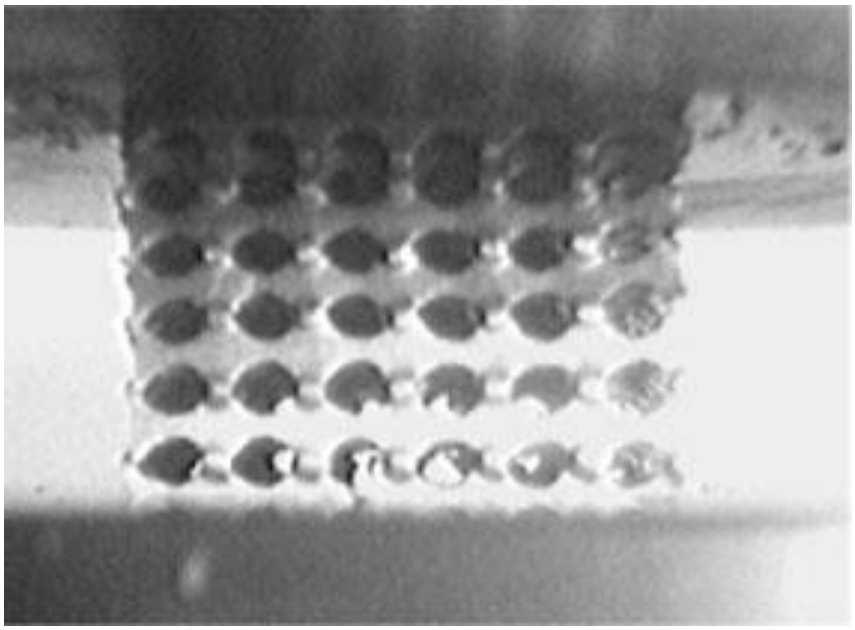


Figure 12- Picture showing buckling process at the walls between holes.

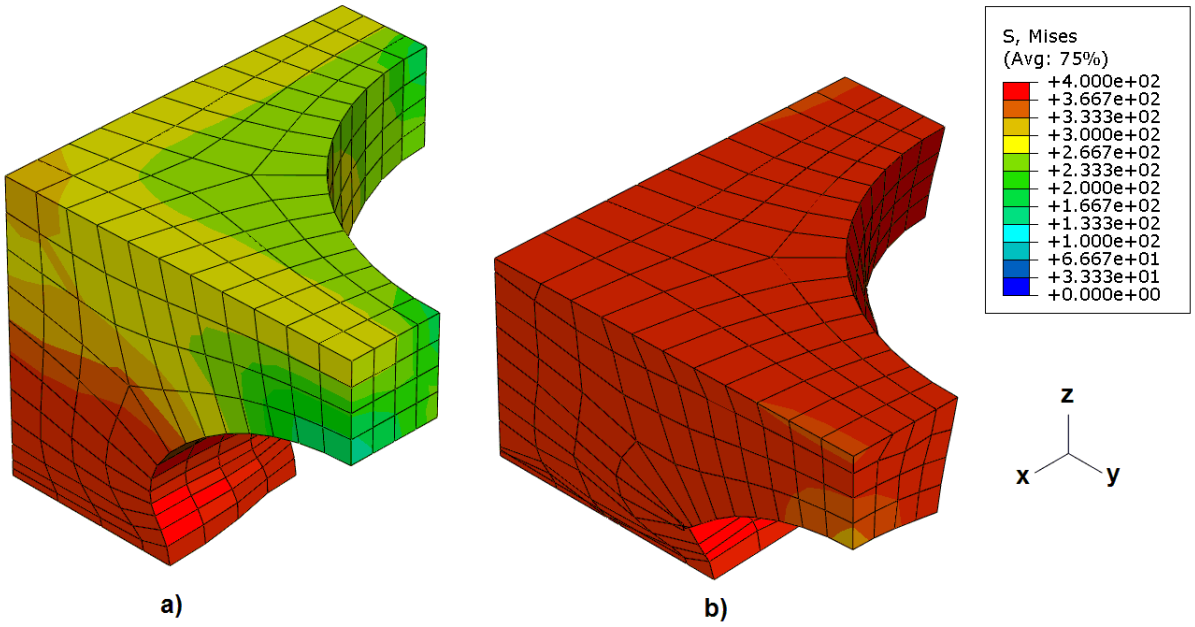


Figure 13- Distribution of von Mises stress (MPa) for a unit cell with MPC (unit cell BCK-0) for an applied macroscopic strain of a)25% b)50%.

The second type of unit cell analyzed, the unit cell BCK-2 and the 2-cells model (Fig. 10-b) are the same, due to the symmetry applied to the unit cell, that represents an eighth of the 2-cells model. They underestimate the stiffness of the cube because in this case all the walls suffer strong buckling effects, that in the actual behavior of the real specimen (Fig. 5) is restricted (at this loading level) to the slenderer external walls. Figure 14 shows the von Mises stress distribution for the unit cell BCK-2 without MPC and Fig. 15 for the 2-cells model. In both cases an applied macroscopic strain of 25% and 50% is shown. In the figures, the axe *z* defines the load direction.

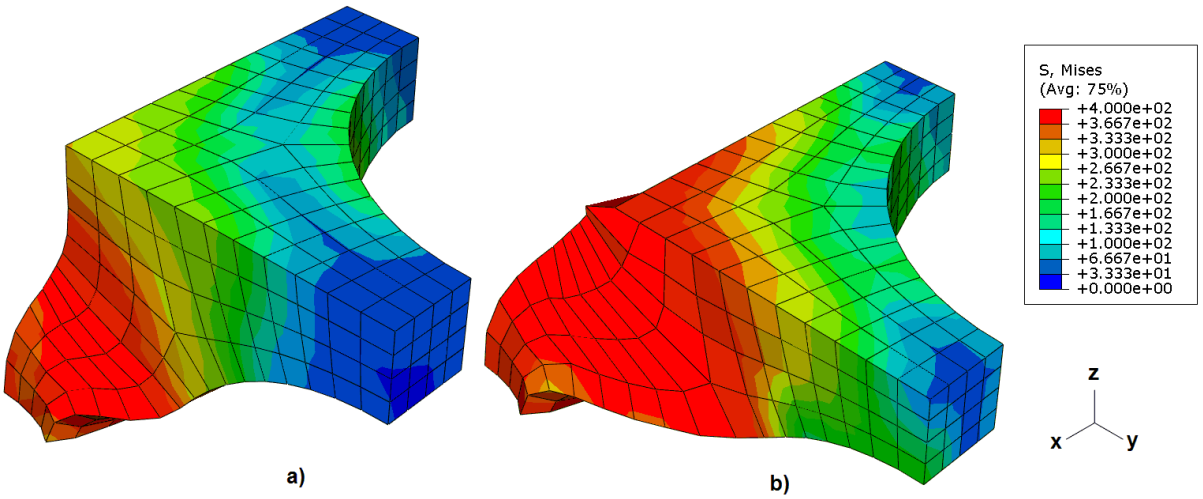


Figure 14- Distribution of von Mises stress (MPa) for a unit cell without MPC (unit cell BCK-2) for an applied macroscopic strain of a)25% b)50%.

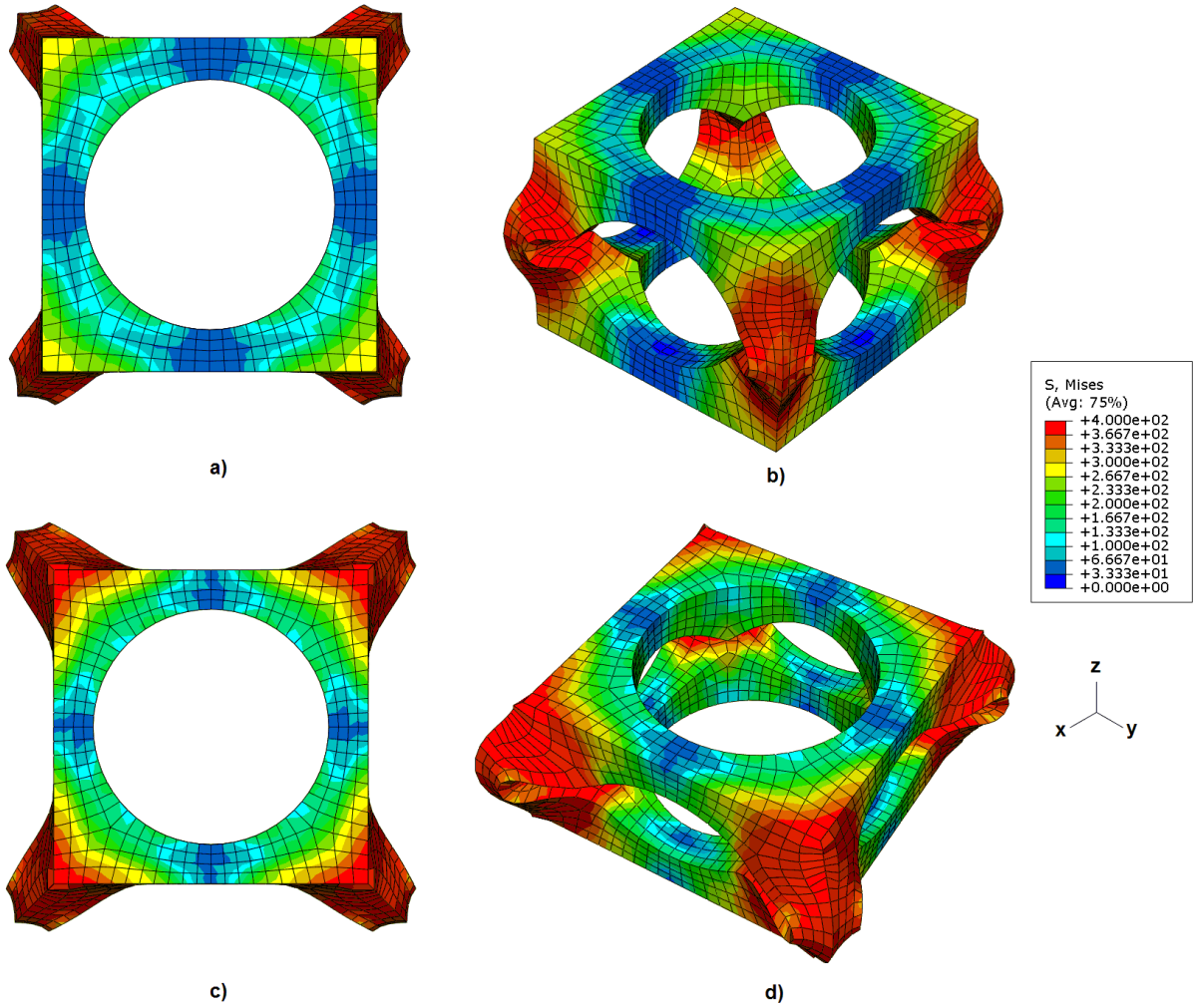


Figure 15- Distribution of von Mises stress (MPa) for a 2-unit cells for an applied macroscopic strain of b)25% d)50%. an their respective top views a) and c).

The other unit cell, with MPC applied just to one face (unit cell BCK-1) is shown in Fig. 16. This one have a behavior next to the unit cell BCK-2 but a little more hard in compression, due to only one wall suffers strong buckling effects and the other remains vertical.

For the 4-units cell, that represent more appropriately the effect of the bucking at the walls between holes, numerical results are closer to the expected real results. The 4-cells is obtained using symmetry conditions. Only a fourth part of the specimen is analyzed.

Figures 17 shows von Mises stress distribution to the 4-cells model at and applied strain of 25% (Fig. 17-a) and 50% (Fig. 17-b). Figure 18 shows the same von Mises distributions in a reflected assemble top view, where the overall view is improved. It is possible to observe there that the buckling of the external wall is properly represented.

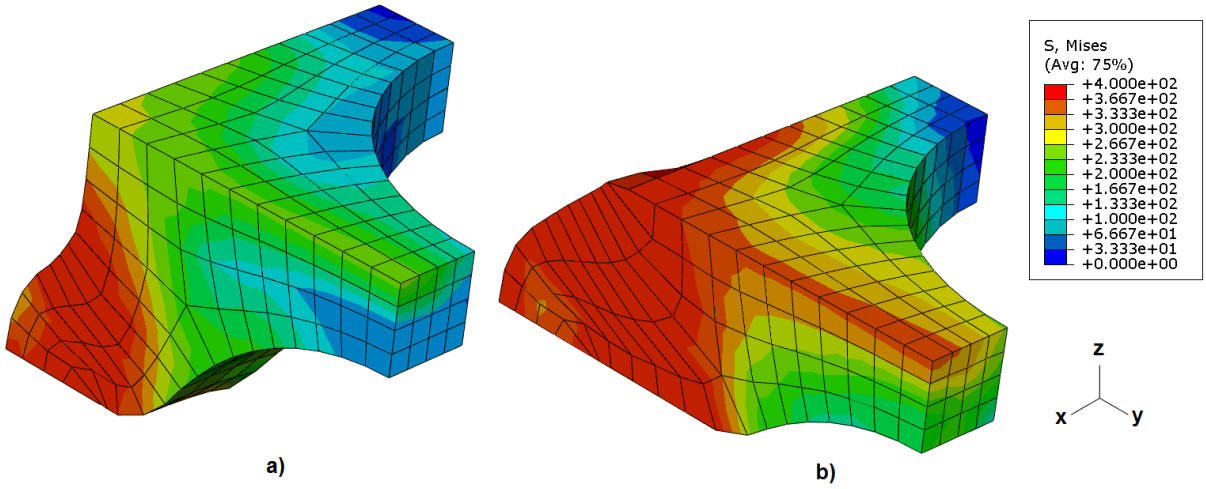


Figure 16- Distribution of von Mises stress (MPa) for a unit cell with MPC (unit cell BCK-1) for an applied macroscopic strain of a)25% b)50%.

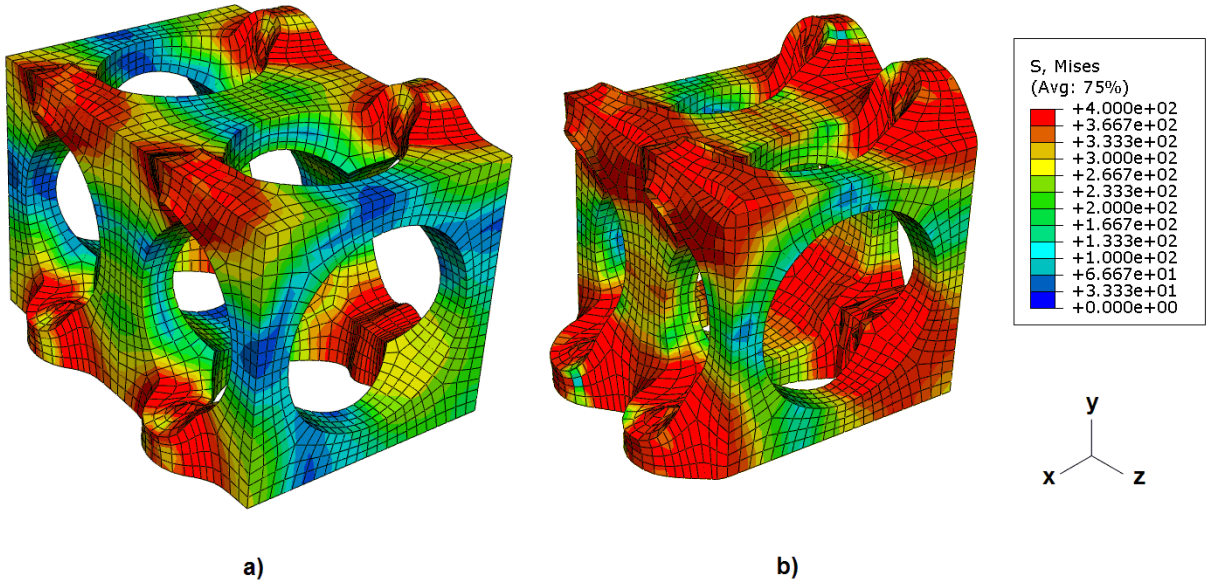


Figure 17- Distribution of von Mises stress (MPa) in a fourth part of a 4-unit cells for an applied macroscopic strain of a)25% b)50%.

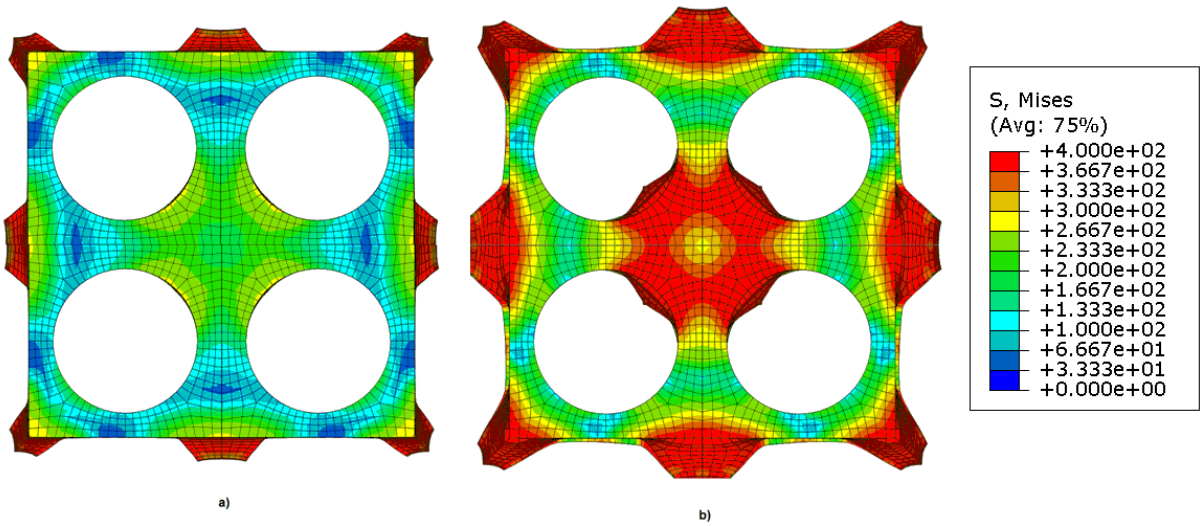


Figure 18- Reflected assemble of top view distribution of von Mises stress (MPa) for a 4-unit cell for an applied macroscopic strain of a)25% b)50%.

4.1 Generalization of the buckling effects on the cellular metal

The analysis of the behavior of the cellular metals under compression shows that each cell than compose the complete structure, can only have 3 different types of buckling effects. The unit cells can have a total buckling effect, like the behavior observed in the unit cell BCK-2 (Fig. 14), a partial buckling effect like the unit cell BCK-1 (Fig. 16) or no buckling effects like the unit cell BCK-0 (Fig. 13). All these effects can be observed in the 4-unit cells compression simulation (Fig. 17 and 18). The most outward cells in the corners of the structure have stronger buckling effects in two directions because there are no restrictions that unable the deformations. The outward cells between the corners of the structure have a unidirectional buckling effect because there is one degree of freedom restricted in this configuration. The internal cells have all degrees of freedom restricted, and no buckling effects occur.

The interpretation of the stress-strain plots for the models used in the analysis (Fig. 11) is that between the two extreme cases, without buckling, and with total buckling effects, there is an intermediary case representing a specimen with certain number of cells. Accepting that only the 3 types of deformation proposed govern the overall behavior of the cellular metal, the number of unit cells and their respectively type of buckling effect are needed to characterize the overall behavior. If their effects are a linear combination at every strain point ε^i for all i unit cells, the stress for a $\sigma_n(\varepsilon)$ number of cells geometry as function of the strain $\sigma_n(\varepsilon)$ is given by

$$\sigma_n(\varepsilon)=\frac{n_2\sigma_2(\varepsilon)+n_1\sigma_1(\varepsilon)+n_0\sigma_0(\varepsilon)}{n_2+n_1+n_0}. \tag{23}$$

where n_2, n_1 and n_0 are the number of cells with a BCK-2, BCK-1 and BCK-0 type of buckling effect, respectively, and $\sigma_2(\varepsilon)$, $\sigma_1(\varepsilon)$ and $\sigma_0(\varepsilon)$ are the stress value for a determined strain ε in each of this type of cells, respectively too. The sum in the denominator is also substituted by the number of cells in the structure, n.

To simplify the application of Eq. (23), the concept of Representative Unit Cells, (also called RUC here) is used. A group of unit cells is chosen to represent the symmetry of the cellular structure, wherein all the other unit cells in the structure may be generated by translations of the representative unit cell integral distances along each of the its edges. Thus, the RUC is the basic structural unit or building block of the cellular structure and defines its behavior by virtue of its geometry and located buckling effects positions. A similarly approach is used in an atomic and crystalline structure order analysis for the metals (Callister, 1990).

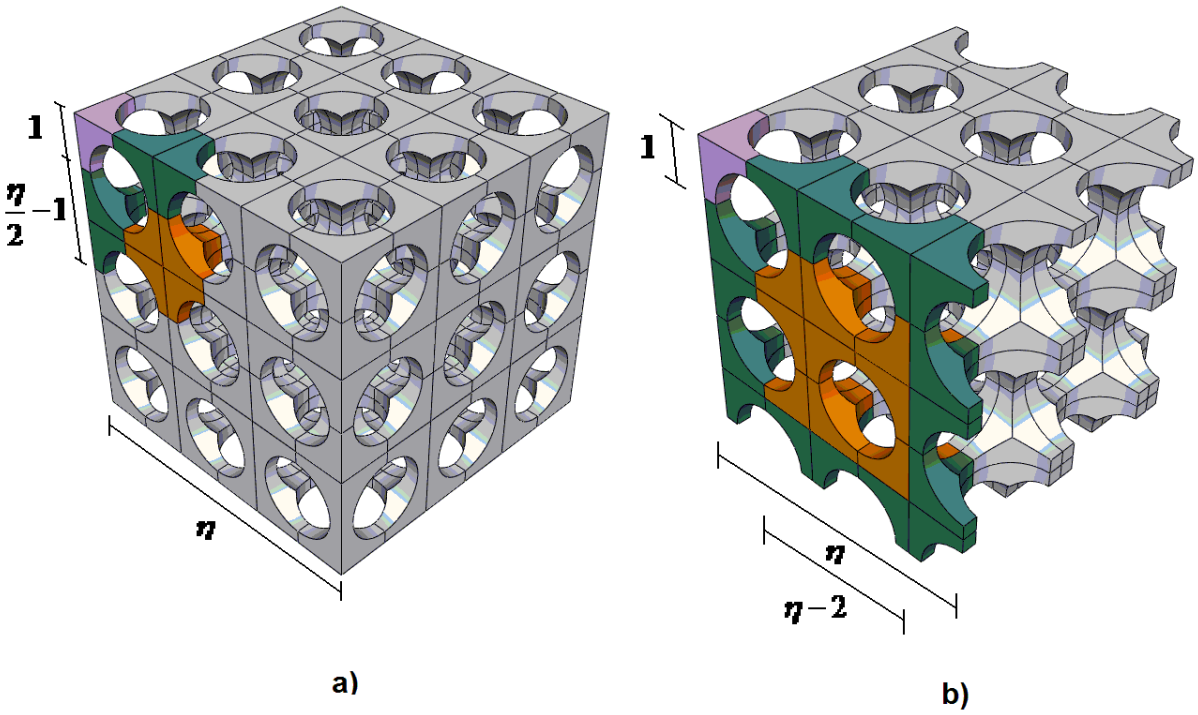


Figure 19- Parameters used to determine the RUC configuration on an a)odd structure (closed) b)even structure (open).

The determination of the RUC is made for a cellular metal with the same number of unit cells η in all the directions. There are two different cases: a geometry where the number η is odd, called closed, and where the number is even, called open.

Figure 19 shows the parameters used to determine the RUC in both cases. The RUC can be represented as a function of the number of each type of buckling effects at every unit cell in the structure

$$RUC = \begin{Bmatrix} n_2 \\ n_1 \\ n_0 \end{Bmatrix}. \tag{24}$$

$$N = n_2 + n_1 + n_0 . \tag{25}$$

and the sum of the number of these unit cells analyzed are N. An important difference between N and n is that the first is the number of cells needed to be analyzed with the concept of RUC, which is smaller than the number of total unit cells in the structure, n.

According to Fig. 19, the Eq. (24) and Eq. (25) can be substituted by

$$RUC^{2\eta} = \begin{Bmatrix} 1 \\ \eta - 2 \\ \left(\frac{\eta}{2} - 1\right)^2 \end{Bmatrix}. \tag{26}$$

$$N^{2\eta} = \frac{\eta^2}{4}. \tag{27}$$

$$RUC^{2\eta-1} = \begin{Bmatrix} 1 \\ 4\eta - 5 \\ (\eta - 2)^2 \end{Bmatrix}. \tag{28}$$

$$N^{2\eta-1} = \eta^2. \tag{29}$$

where the 2η indicator symbolizes an odd structure and a $2\eta - 1$ is used for an even number of cells structure. These terms can be substituted in Eq. (23), resulting

$$\sigma_n(\varepsilon)^{2\eta} = 4\left[\frac{\sigma_2(\varepsilon) + (\eta - 2)\sigma_1(\varepsilon) + \left(\frac{\eta}{2} - 1\right)^2 \sigma_0(\varepsilon)}{\eta^2}\right]. \tag{30}$$

$$\sigma_n(\varepsilon)^{2\eta-1} = \frac{\sigma_2(\varepsilon) + (4\eta - 5)\sigma_1(\varepsilon) + (\eta - 2)^2 \sigma_0(\varepsilon)}{\eta^2}. \tag{31}$$

These equations establish the relation between the stress and the number of cells in each direction in function of the strain.

The limit cases

$$\lim_{n\to\infty} \sigma_n(\varepsilon) = \sigma_0(\varepsilon). \tag{32}$$

$$\lim_{n\to 1} \sigma_n(\varepsilon) = \sigma_2(\varepsilon). \tag{33}$$

represent the behavior of two unit cells chosen as the limit cases, the unit cell BCK-0 and the unit cell BCK-2, and are in agreement with the initial proposal.

Figure 20 shows stress-strain plots for cellular metals with different number of cells generated with Eq. (30) and Eq. (31).

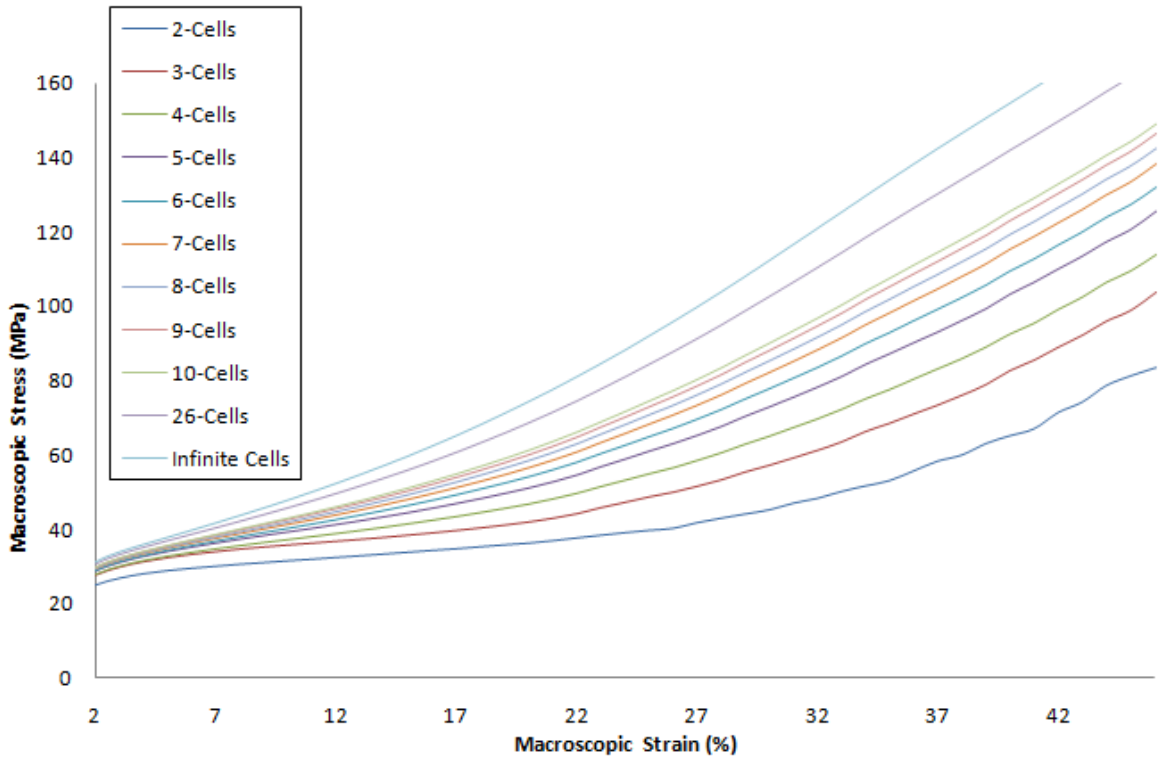


Figure 20- Stress strain plots for different number of cells generated with Eq. (30) and Eq. (31).

The curves of Fig. 19 show that with the enlargement of the number of cells the buckling effect decrease, conducing to a behavior next to the unit cell BCK-0. The 4-cells unit compression test simulation has the same results found with the application of the Eq. (30) and Eq. (31).

5. FINAL COMMENTS

This paper presents some new results from a research in development (Oliveira et al., 2008, 2007 and 2006).

It is shown that the contact hypothesis and the generalization model based on the study of the internal buckling effects acting in the structure are valid. The use of more experimental results should be needed to confirm this analysis. The research will continue the study, with the application of dynamic analysis and a more complex generalization of the geometry of the structure.

Acknowledgements

We thank CNPq, CAPES and GRICES for financial support thought the CAPES/GRICES program (Proc. 127/05) and PROPESQ-UFRGS for continuous support of our research projects.

REFERENCES

ABAQUS, 1992. *Theory Manual v. 5.2*, Providence, USA: Hibbit, Karlsson & Sorensen, Inc. Callister W. D., 1990. Fundamentals of Materials Science and Engineering. John Wiley & Sons.

Chu C.C. and Needleman A., 1980. Void nucleation effects in biaxially stretched sheets. *ASME Journal of Engineering Materials and Technology*, vol. 102, pp. 249-256.

Cunda L.A.B. and Creus G.J., 1999. A note on damage analyses in process with nonmonotonic loading. *Computer Modeling and Simulation in Engineering,* Vol. 4, pp. 300-303.

Cunda L.A.B., Öchsner A., Creus G.J., 2005. Damage in metallic foams. In *Proceedings of the XXVII Iberian Latin-American Congress on Computational Methods in Engineering – CILAMCE 2005*.

Gurson A.L., 1977. Continuum theory of ductile rupture by void nucleation and growth: part I-yield criteria and flow rules for porous ductile media. *ASME Journal of Engineering Materials and Technology*, vol. 99, pp. 2-15.

Munoz-Rojas P.A.. Fiedler T., Cunda L.A.B., Öchsner A., Creus G.J., 2007. Parameter Identification to Simulate a Traction Test Applying Gurson Damage Model. In *Proceedings of the CMNE 2007 – Congress on Numerical Methods in Engineering/ CILAMCE 2007 – XXVIII Latin-American Congress on Computational Methods in Engineering*.

Öchsner A., Lamprecht K., 2003. On the uniaxial compression behavior of regular shaped cellular metals. *Mechanics Research Communications*, vol. 30, pp. 573-579.

Öchsner A., Winter W. and Kuhn G., 2003. On an elastic-plastic transition zone in cellular metals. *Archive of Applied Mechanics,* vol. 73, pp. 261-269.

Oliveira, B.F. Cunda L.A.B, Öchsner A., Creus G.J, 2008. Comparison between RVE and full mesh approaches for the simulation of compression tests on cellular metals. *Materialwissenschaft und Werkstofftechnik*, vol. 39, n. 2, pp. 133-138.

Oliveira B.F., Cunda L.A.B, Öchsner A., Creus G.J., 2007. Finite element simulation of compression tests on cellular metals. In *Proceedings of the XXVIII Iberian Latin-American Confress on Computational Methods in Engineering – CILAMCE 2007*.

Oliveira B.F., Cunda L.A.B, Öchsner A., Creus G.J., 2006. Gurson damage model: applications to case studies. In *Proceedings of the XXVII Iberian Latin-American Confress on Computational Methods in Engineering – CILAMCE 2006.*

Tvergaard V., 1981. Influence of voids on shear band instabilities under plane strain conditions. *International Journal of Fracture,* vol. 17, pp. 389-407.

Tvergaard V., 1982. Material failure by void coalescence in localized shear bands. *International Journal of Solids and Structures,* vol. 18, pp. 659-672, (1982).